APPLICATION NOTE

Automated single cell tracking using the Operetta high-content analysis system: Analyzing chemokinesis of cancer cells.

Key features

- Automated single cell tracking using Harmony® software
- Digital phase imaging to avoid phototoxicity
- Multiparametric analysis of cell morphology using TIBCO Spotfire

For research use only.
Not for use in diagnostic procedures.

Background

Cell migration is an essential component of metastatic dissemination of tumor cells from the primary tumor to local and distant sites. For many types of cancer, cancer cells respond to stimulation with growth factors or chemokines with an increased migration – a process called chemokinesis. Consequently, pathways which render tumor cells susceptible to chemokinesis are interesting drug targets for reducing the risk of metastasis in cancer patients [Roussos et al., 2011].

Endothelial Growth Factor (EGF) stimulates the cell migration in various types of cancer including, but not limited to, breast cancer, glioma and non-small cell lung cancer (NSCLC) [Caino et al., 2012; Pickhard et al., 2011; Price et al., 1999]. The signaling pathway involves activation of phospholipase Cγ (PLCγ), protein kinase C (PKC) and cofilin, of which the latter might be involved in regulating the directionality of the migration [Caino et al., 2012; Wang et al., 2007]. EGF can be released from tumor-associated macrophages, providing a paracrine stimulation of migration and even a chemotactic guidance of cells towards blood vessels [Mouneimne et al., 2004; Roussos et al., 2011].

Here, we present a high-content screening application for analyzing the cell migration of NSCLC cells in a live cell assay. Using the Operetta® high-content analysis system and digital phase contrast imaging, we tracked migrating cancer cells using automated single cell tracking in the Harmony® high-content imaging and analysis software.

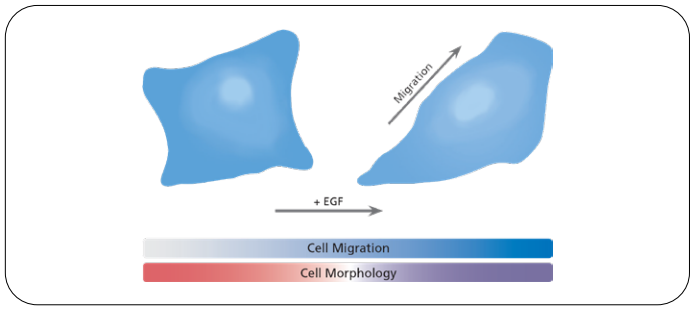

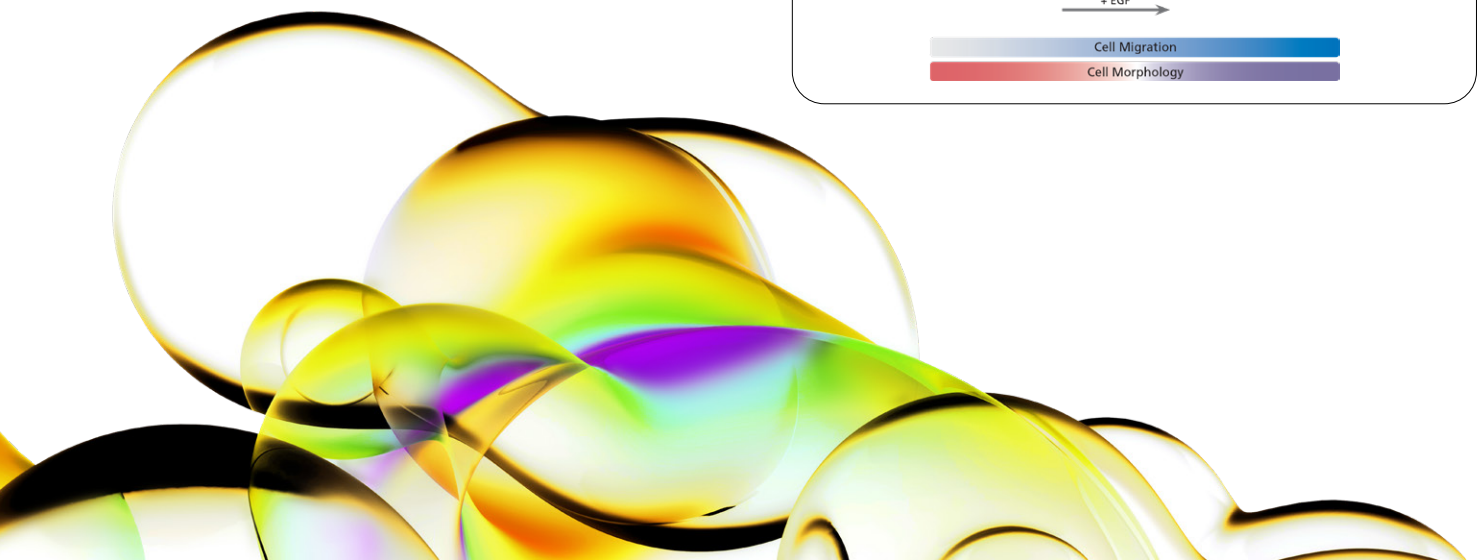

Application

A549 non-small cell lung cancer cells were cultured in F12-HAM (Sigma-Aldirch) supplied with 10% FCS and 2 mM L-Glutamine. To perform the assay, cells were seeded in serum-free medium at a density of 4500 cells per well into a 384-well CellCarrier™ microplate (Revvity, 6007558) freshly coated with 5 µg/cm^2 collagen I (BD Biosciences, 354236). After overnight cultivation, cell migration was stimulated by addition of EGF (Sigma-Aldrich, E9644) at different concentrations or by addition of 100 nM phorbol 12-myristate 13-acetate (PMA) (Sigma-Aldrich, P1585). In the presence of 100 ng/mL EGF, the following inhibitory compounds were tested: AG-1478 (Cayman Chemicals, 10010244), Nocodazol (Sigma-Aldrich, M1404) and Cytochalasin D (Sigma-Aldrich, C8273).

Live cell imaging was performed using an Operetta high-content analysis system equipped with a temperature and CO_2 control option (TCO) set to 37 °C and 5% CO_2. Directly after addition of the compounds, microplates were placed onto the pre-heated Operetta system and incubated for 30 min. After incubation, digital phase contrast images were acquired at 10X magnification (10X high NA objective) using Operetta's automatic digital phase contrast algorithm. Phototoxicity is minimized because digital phase imaging uses a red light LED transmission light source. To analyze the morphology of migrating cells in detail, we acquired digital phase contrast images using a 20X high NA objective. Images were acquired for up to 6 h at imaging intervals of 5-15 min.

Images were segmented using the *Find Cells* building block of the Harmony software, which provides a dedicated algorithm for segmenting digital phase contrast images. The segmented cells were subjected to cell tracking using the *Track Objects* building block. We calculated different properties that describe cell migration either on a per time point basis such as *Current Speed* or on a per cell track basis such as *Displacement*. Displacement is the direct line between the position of the first observation of a cell and the position of the last observation of a cell. This proved to be the most valuable readout for describing cell migration.

Optimization of image acquisition

Live cell imaging can result in a large number of images, especially when short imaging intervals are used to ensure accurate cell tracking. For this reason, we optimized the imaging interval to identify the longest imaging interval that provided robust cell tracking. Similarly, we optimized the total imaging duration.

These optimization studies were based on a migration experiment depicted in Figure 1, in which cells were stimulated to migrate by a treatment with 100 ng/mL EGF. The videos generated by the Harmony software showed an increased cell migration after stimulation with EGF, as indicated by the length of the cell tracks. Using this measurement, we tested how extending the interval between two consecutive images (imaging interval) *in silico* impacts on the primary readout value cell displacement. To this end, we considered either every time point for the analysis or only every second, every third, every fourth, and so on (Figure 2). We then plotted the cell displacement and the Z′ factor against the imaging interval. As panel 2B illustrates, extending the imaging interval beyond 15 min strongly impairs the Z′ factor due to a decrease in the cell displacement. This can be explained by cells moving too far between two images to be correctly tracked. Consequently, long tracks are split into two or more shorter tracks that have a much smaller displacement than the longer original cell track resulting in a decreased average cell displacement per well.

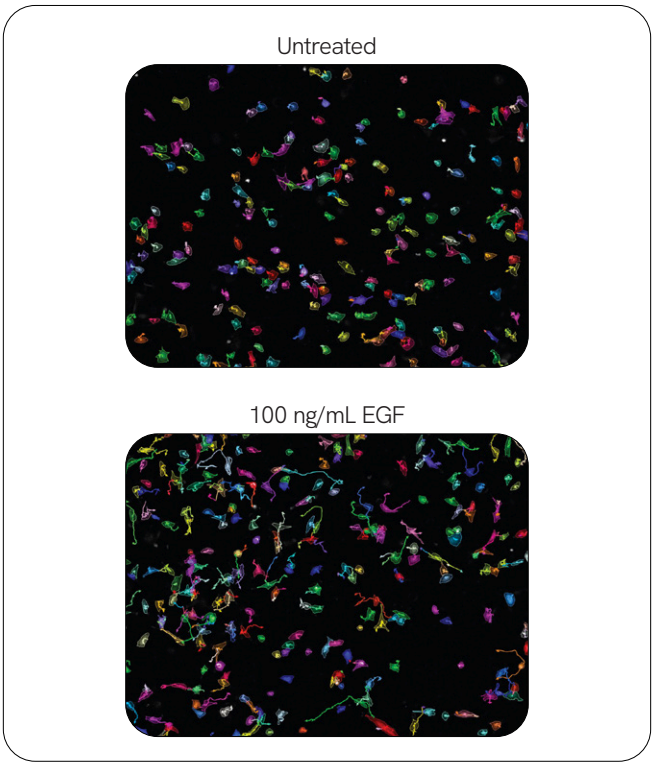

Figure 1: Induction of cell migration of A549 non-small cell lung cancer cells. Images are snapshots from videos generated by the Harmony software showing digital phase contrast images with the segmentation mask and the cell track overlaid. Untreated, serum starved cells show little or almost no cell migration as indicated by short cell tracks. Treatment with 100 ng/mL EGF significantly increases cell migration and the obtained cell tracks are much longer.

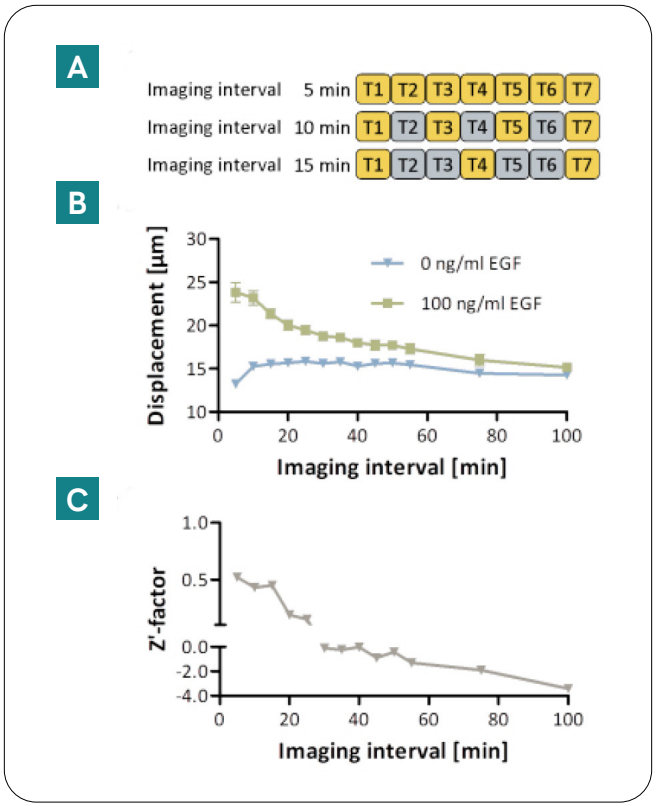

Figure 2: Optimization of the imaging interval. (A) Starting from a measurement with an imaging interval of 5 min, the number of time points considered for analysis was reduced by leaving out an increasing number of time points. Thereby, the imaging interval was stepwise increased *in silico*. (B) With increasing imaging interval, the measured displacement of EGF-stimulated cells decreases and approaches the displacement seen for non-stimulated cells. This decrease is due to a lack of overlap between adjacent time points for fast migrating cells, resulting in failed tracking for fast cells. (C) With the displacement of stimulated cells approaching the displacement of non-stimulated cells, the calculated Z′ significantly decreases. An excellent Z′ is achieved with an imaging interval of no greater than 15 min. n=5 wells, error bars depict standard deviation.

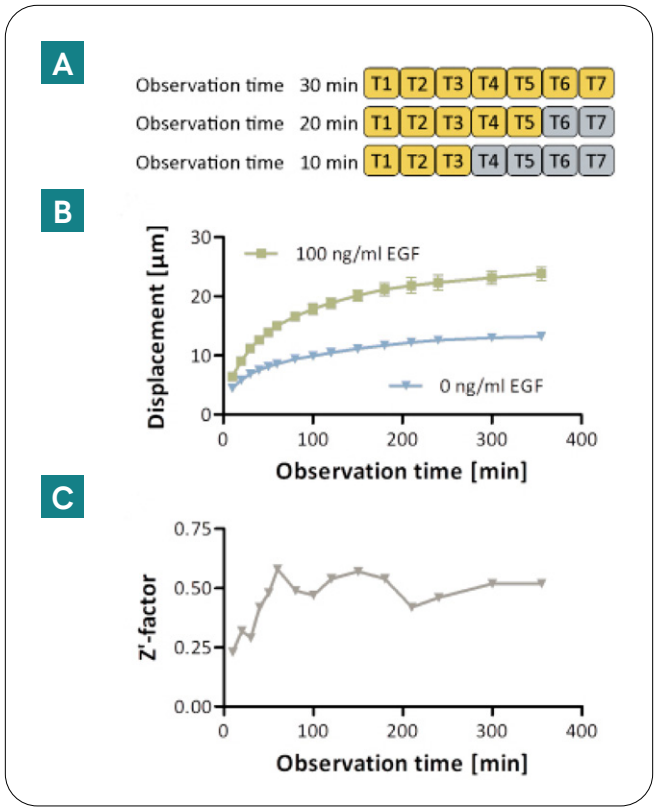

Figure 3: Optimization of the observation time. (A) Starting from a measurement with an imaging interval of 5 min, the number of time points considered for analysis was reduced by excluding an increasing number of time points from the end of the time series. Thereby, the observation time was stepwise reduced in *silico*. (B) With an increasing observation time, the measured displacement of EGF-stimulated cells increases as the cells have more time to migrate. (C) With the increasing difference between the treated and untreated cells, the calculated Z′ significantly increases. An excellent Z′ is achieved with an observation time of at least 60 min. n=5 wells, error bars depict standard deviation.

Using a similar approach, we tested how long we had to image the cells in total to obtain a good Z′ factor. To this end, we considered either every time point for the analysis or only the first 60 time points, only the first 50 time points, and so on (Figure 3). Thereby, we decreased the total observation time *in silico*. Again, we plotted the displacement and the corresponding Z′ factor against the observation time. The obtained Z′ factor increased with the observation time, up to approximately 60 min before it becomes more or less constant at above 0.5. This finding can be explained by the increase in the difference of the displacement of EGF-treated and untreated cells. This means that imaging the cells longer than 60 min does not result in a significant improvement of the assay window.

In summary, the optimization of the image acquisition settings revealed that an imaging interval of 15 min and a total observation time of approximately 60 min are sufficient to reach an excellent Z′ of around 0.5. Based on these optimized imaging parameters, it is possible to run a full kinetic assay on an entire 384-well plate with 1 image field per well in 75 min.

Effects of compound treatment on cell migration

EGF-stimulated migration of A549 cancer cells can be influenced in a positive or negative way by different compounds (Figure 4). Initially, we tested two unspecific inhibitors of cell migration, Nocodazole and Cytochalasine D, and the unspecific agonist PMA. Nocodazole inhibits cell migration by interfering with microtubule dynamics, whereas Cytochalasin D inhibits actin polymerization causing a reduction in cell motility. In contrast, PMA activates protein kinase C resulting in a stimulation of cell migration. Figure 4 shows the quantitative analysis of cell migration assessed by cell displacement. Treatment with 100 nM PMA clearly stimulates cell migration to a similar level as induction by 100 ng/mL EGF. Treating cells with 200 nM Nocodazole or 100 nM Cytochalasin D in the presence of 100 ng/mL EGF results in a significant reduction of cell displacement.

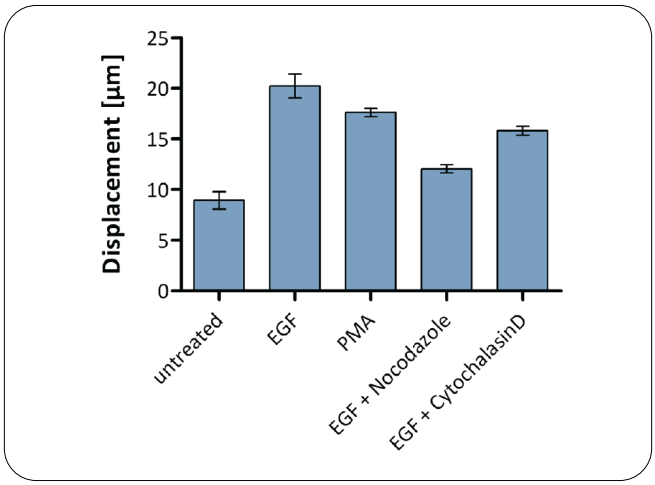

Figure 4: Compound treatment of A549 NSCLC cells. Serum-starved cells were treated with 100 ng/mL EGF, 100 nM PMA, 100 ng/mL EGF in combination with 200 nM Nocodazole or 100 ng/mL EGF in combination with 100 nM Cytochalasin D. n=4 wells, error bars depict standard deviation.

In a more detailed study, we acquired a full dose-response curve of the EGF-induced cell migration. We found a dose-dependent increase in cell migration with a calculated EC_{50} for EGF of 2.7 ng/mL (Figure 5). In the next step, we treated the cells with different concentrations of AG-1478, which is an EGF receptor tyrosine kinase inhibitor that exhibits antitumor activity [Johns et al., 2003]. In the presence of 100 ng/mL EGF, we observed a dose-dependent decrease of cell displacement with increasing concentrations of AG-1478 (Figure 5). The calculated IC_{50} was 1.5 µM, which is in line with previously published data [Han et al., 1996].

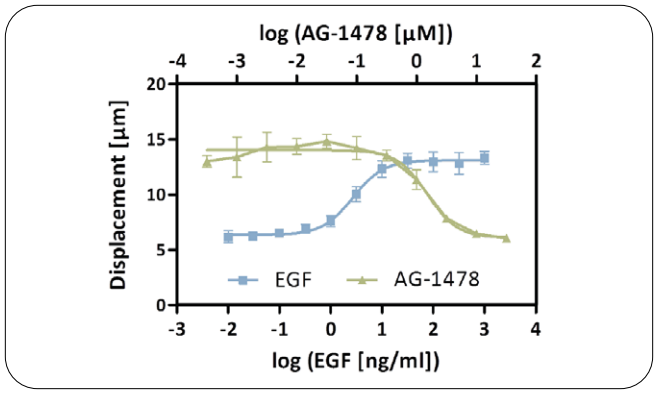

Figure 5: Dose-response curves for EGF and AG-1478. Serum-starved cells were treated with increasing concentrations of EGF. A dose-dependent increase in cell migration was observed with a calculated EC_{50} of 2.7 ng/mL (blue curve). In the presence of 100 ng/mL EGF, cells were treated with increasing concentrations of the tyrosine kinase inhibitor AG-1478. As dose-dependent decrease in cell migration was observed with a calculated IC_{50} of 1.5 µM (green curve). n=4 wells, error bars depict standard deviation.

Morphological profiling of migrating cells

Single cell tracking provides time-resolved single cell data, so morphological properties of migrating cells can be extracted from any time point. We were interested to see whether it was possible to identify different phenotypes that correlate with different cell motilities. To obtain morphological profiles of migrating cells, we acquired digital phase contrast images of EGF-treated cells using a 20X high NA objective. Using the building blocks of the Harmony software, we extracted 45 morphological properties ranging from simple properties like cell area and cell roundness to complex properties like membrane ruffliness (i.e. texture analysis of a small membrane region). The numerical data obtained was subsequently transferred to TIBCO Spotfire®, which facilitates the analysis of large multiparametric datasets. Within TIBCO Spotfire, we used hierarchical clustering to group the cells based on their morphology at any of the time points (approx. 32,000 data points). In total, we obtained 23 clusters and analyzed 5 in more detail as they comprised 75% of all data points (Figure 6A). To determine the current speed of a cell at any time point, noise from short time scale movement was filtered to focus on more persistent movement. We found significant differences in the speed between the different clusters (Figure 6B), indicating that fast migrating cells share a common morphology. Figure 6C shows a panel of representative cells for each cluster. Whereas cluster 24 contains mainly small and round cells that have a very low speed, the fast migrating cells in cluster 38 have pronounced membrane ruffles.

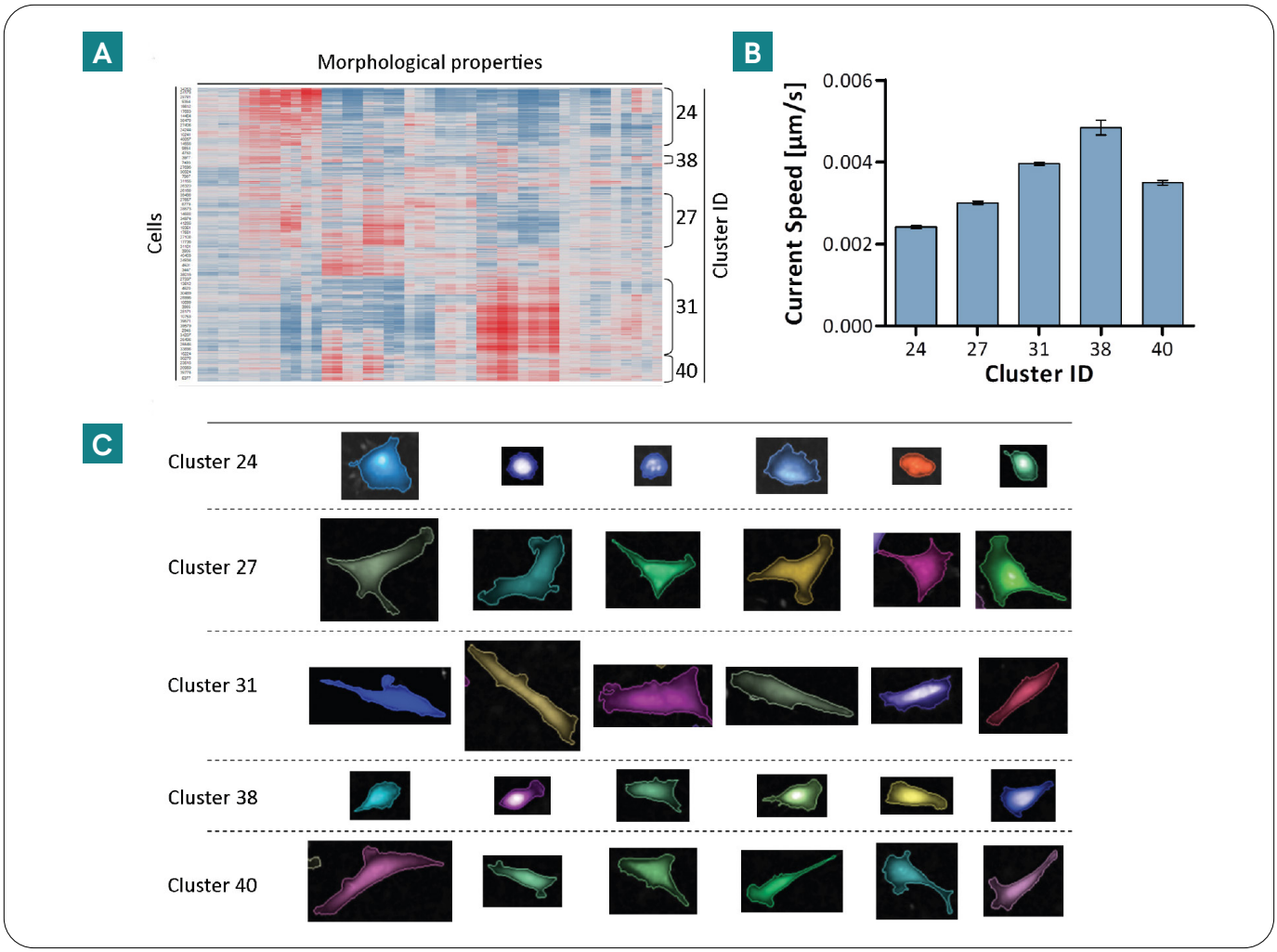

Figure 6: Morphological profiling of migrating cells. (A) Heatmap obtained by hierarchical clustering in TIBCO Spotfire. The heatmap reflects 45 properties for 32,000 cells. Cells were grouped into 23 clusters based on the similarity of their morphological profile and the five clusters annotated on the right were investigated in more detail. (B) Mean current speed over all cells in a cluster. The clusters comprise different cell numbers. Cluster 24: 6237 cells; cluster 27: 5718 cells; cluster 31: 8159 cells; cluster 38: 647 cells; cluster 40: 2936 cells. Error bars depict standard error of the mean. (C) Representative selection of cells from each cluster. All cell images are shown at the same magnification.

Conclusions

In this study, we have shown how a combination of digital phase contrast imaging and automated single cell tracking can be used to study cell migration in a live cell assay. Using the Operetta high-content analysis system equipped with a temperature and CO_2 control option (TCO), optimal cell viability was maintained throughout the entire observation time. Additionally, the red light LED that is used to generate the digital phase images minimizes phototoxicity. This setting allows for dynamic processes in cells to be studied without biasing the results by the observation process itself.

Since the workflow is based on the easy-to-use building blocks of the Harmony software, setting up object tracking in the Harmony software is almost as simple as setting up a standard image analysis sequence as it follows the same workflow-based approach. By combining object tracking with other building blocks, a variety of properties can be obtained that not only describe cell motion but also provide time-resolved single object data on intensities, cell morphology or texture. Generally speaking, this compensates for the cell-to-cell variation in response to compound treatment similar to what we have shown in previous studies [Fassler et al., 2012], leading to robust assays statistics with Z'-scores above 0.5.

The easy transfer of numerical data from the Harmony software into TIBCO Spotfire facilitates the analysis of large data sets which are typically the result of entire high-content screens. TIBCO Spotfire provides tools like hierarchical clustering or principal component analysis that are very powerful when working with multiparametric data. As we have demonstrated in our study, these tools can be used to create a morphological profile of migrating cells and details on the mode of action of a certain migration inhibitor can be revealed. This kind of additional information is not available in conventional migration assays such as the scratch assay.

In summary, the flexible acquisition of fluorescence and digital phase contrast images using the Operetta high-content analysis system and the building block-based analysis of the Harmony software provided easy-to-use tools to set up automated single cell tracking without requiring expert knowledge.

References

Caino, M.C., Lopez-Haber, C., Kissil, J.L., and Kazanietz, M.G. (2012): Non-small cell lung carcinoma cell motility, rac activation and metastatic dissemination are mediated by protein kinase C epsilon. *PloS One*, 7 (2), e31714.

Fassler, M., Karassina, N., Benink, H., Kirsch, A., Preckel, H., Cong, M., and Boettcher, K. (2012): Quantification of NF-kB signaling in living cells: A high-content workflow for the generation of timeresolved single-cell data. *Scientific Poster*.

Han, Y., Caday, C.G., Nanda, A., Cavenee, W.K., and Huang, H.J. (1996): Tyrphostin AG 1478 preferentially inhibits human glioma cells expressing truncated rather than wild-type epidermal growth factor receptors. *Cancer Research*, 56 (17), 3859–61.

Johns, T.G., Luwor, R.B., Murone, C., Walker, F., Weinstock, J., Vitali, A.A., Perera, R.M., Jungbluth, A.A., Stockert, E., Old, L.J., Nice, E.C., Burgess, A.W., and Scott, A.M. (2003): Antitumor efficacy of cytotoxic drugs and the monoclonal antibody 806 is enhanced by the EGF receptor inhibitor AG1478. *Proceedings of the National Academy of Sciences of the United States of America*, 100 (26), 15871–6.

Mouneimne, G., Soon, L., DesMarais, V., Sidani, M., Song, X., Yip, S.-C., Ghosh, M., Eddy, R., Backer, J.M., and Condeelis, J. (2004): Phospholipase C and cofilin are required for carcinoma cell directionality in response to EGF stimulation. *The Journal of Cell Biology*, 166 (5), 697–708.

Pickhard, A.C., Margraf, J., Knopf, A., Stark, T., Piontek, G., Beck, C., Boulesteix, A.-L., Scherer, E.Q., Pigorsch, S., Schlegel, J., Arnold, W., and Reiter, R. (2011): Inhibition of radiation induced migration of human head and neck squamous cell carcinoma cells by blocking of EGF receptor pathways. *BMC Cancer*, 11, 388.

Price, J.T., Tiganis, T., Agarwal, A., Djakiew, D., and Thompson, E.W. (1999): Epidermal growth factor promotes MDA-MB-231 breast cancer cell migration through a phosphatidylinositol 3′-kinase and phospholipase C-dependent mechanism. *Cancer Research*, 59 (21), 5475–8.

Roussos, E.T., Condeelis, J.S., and Patsialou, A. (2011): Chemotaxis in cancer. *Nature Reviews. Cancer*, 11 (8), 573–87.

Wang, W., Eddy, R., and Condeelis, J. (2007): The cofilin pathway in breast cancer invasion and metastasis. *Nature Reviews. Cancer*, 7 (6), 429–40.

Authors

Matthias Fassler
Karin Boettcher
Hartwig Preckel

Revvity, Inc.

Revvity, Inc.
940 Winter Street
Waltham, MA 02451 USA
www.revvity.com

For a complete listing of our global offices, visit www.revvity.com
Copyright ©2023, Revvity, Inc. All rights reserved.